



Birkbeck ePrints: an open access repository of the research output of Birkbeck College

<http://eprints.bbk.ac.uk>

Betson, Mark; Barker, John; Barnes, Paul; Atkinson, Tim and Jupe, Andrew (2004). Porosity imaging in porous media using synchrotron tomographic techniques. *Transport in Porous Media* 57 (2) 203 – 214.

This is an author-produced version of a paper published in *Transport in Porous Media* (ISSN 0169-3913). This version has been peer-reviewed but does not include the final publisher proof corrections, published layout or pagination.

All articles available through Birkbeck ePrints are protected by intellectual property law, including copyright law. Any use made of the contents should comply with the relevant law.

Citation for this version:

Betson, Mark; Barker, John; Barnes, Paul; Atkinson, Tim and Jupe, Andrew (2004). Porosity imaging in porous media using synchrotron tomographic techniques. *London: Birkbeck ePrints*. Available at:

<http://eprints.bbk.ac.uk/archive/00000346>

Citation for the publisher's version:

Betson, Mark; Barker, John; Barnes, Paul; Atkinson, Tim and Jupe, Andrew (2004). Porosity imaging in porous media using synchrotron tomographic techniques. *Transport in Porous Media* 57 (2) 203 – 214.

<http://eprints.bbk.ac.uk>

Contact Birkbeck ePrints at lib-eprints@bbk.ac.uk

POROSITY IMAGING IN POROUS MEDIA USING SYNCHROTRON TOMOGRAPHIC TECHNIQUES

MARK BETSON¹, JOHN BARKER², PAUL BARNES³, TIM ATKINSON²,
ANDREW JUPE³

¹ Environment Systems Group, ADAS, Wergs Road, Wolverhampton, WV6 8TQ.

² Hydrogeology Group, Department of Earth Sciences, UCL, Gower Street,
London, WC1E 6BT.

³ Industrial Materials Group, School of Crystallography, Birkbeck College, Malet
Street, London, WC1E 7HX.

ABSTRACT

This paper describes novel uses of synchrotron radiation in examining porosity distributions within porous media. Tomographic Energy Dispersive Diffraction Imaging (TEDDI) and Tomographic X-Ray Fluorescence (TXRF) have been combined within one measurement method and used to highlight the porosity distribution in a typical sample of English Chalk.

Key words: porosity structure, diffusion, hydrogeology, synchrotron, X-ray, tomography, tracing

1. Introduction

Traditionally the experimental measurements of porosity and diffusion parameters have been performed using column methods, (e.g. Williams and Higgo, 1994) and more recently with remote geophysical techniques, for example X-ray tomography and electrical resistivity (Olsen *et al.*, 1999; Binley *et al.*,

1996a;1996b, Liaw *et al.*, 1996; Reichert *et al.*, 2001). Presented here are new synchrotron X-ray based methodologies for highlighting porosity distributions and tracing solute movement, which are non-destructive and enable different phases to be identified within the experimental sample. In the trial experiments given here uncracked chalk rock is taken as a representative hydrogeological porous medium.

1.1. Tomographic X-Ray Energy Dispersive Diffraction (TEDDI)

The technique, TEDDI, has been developed recently (Hall *et al.* 1998; Barnes *et al.* 2000; Colston *et al.* 2000), finding an exceptionally wide range of applications in materials, chemical and engineering science. TEDDI utilises energy dispersive diffraction (EDD), a less common mode of diffraction in which diffraction patterns are dispersed in photon energy (E) rather than angle (2θ) space. It is well known that in X-ray diffraction the crystal lattice planar spacing (d_{hkl} , where hkl indicates the Miller indices of the plane), the orientation of these planes to the incident photons (θ) and the wavelength (λ) of the radiation are related by Bragg's law:

$$\lambda = 2 d \sin \theta \quad (1)$$

Giessen and Gordon (1968) and Buras *et al.* (1968) recasted Bragg's law into a more convenient form for EDD by means of the Planck-Einstein equation:

$$E = hc / \lambda \quad (2)$$

(h is Plancks constant and c is the speed of light), producing the relation:

$$Ed \sin \theta = 6.1993 \text{ (keV.}\mathring{\text{A}}) \quad (3)$$

X-rays from a synchrotron radiation source contain a broad spectrum of energies of which typically 20-100 keV are detected during *in situ* experiments by means of an energy-dispersive detector multi-channel analyser (MCA) system. The energy calibration of such detectors is normally performed using known energies of fluorescent emissions from various metal foils stimulated by a γ -radiation source.

In energy dispersive diffraction, the detectors are located at fixed scattering angles, 2θ (see Figure 1), selected to maximise the number of useful d-spacing reflections that is compatible with an acceptable loss of intensity through sample absorption (these two factors being opposed to each other in their variation with 2θ); the peak separation and flux versus energy profile of the X-ray beam are additional considerations that might affect the choice of 2θ .

Figure 1

Once set, the 2θ angle is calibrated, using d-spacings from a standard material, such as NIST silica or gypsum, the angle being determined from equation 3. The plots of relative intensity against d-spacing for each pattern can be compared, in terms of peak positions, to those in existing diffraction data sets (such as those provided by the International Center for Diffraction Data, ICDD), although the relative intensities differ from standard patterns collected using conventional angle-scanning diffraction methods.

Combining this system with a well-defined X-ray beam slit system and a motorized x,y,z-translation stage enables the sample to be systematically moved in one (line), two (grid) or three dimensions so that diffraction patterns are

collected from a lozenge-shaped volume (Figure 1) placed at all required positions in the sample; in this way a compositional/structural map of the sample can be assembled based on diffraction information. The resolution of the grid depends on the spacings between the individual spectra and the dimensions of the beam. In particular the spatial resolution along the direction of the incident beam tends to be poorer (i.e. longer) due to severe lengthening of the lozenge when using low 2θ angle (Figure 1).

1.2. Tomographic X-Ray Fluorescence (TXRF)

TXRF is an extension of the TEDDI principle whereby characteristic fluorescence, rather than diffraction, peaks become the prime imaging signal; unlike diffraction peaks, their position in energy is independent of the scattering angle, 2θ . The requirement that only relatively high energy photons will have sufficient penetration (i.e. low absorption) for most *in situ* applications means that only heavier elements ($Z > 40$ for $K\alpha$ fluorescence) are easily detectable in practice. With this in mind caesium, barium and lanthanum were selected for these experiments (e.g. Cs- $K\alpha_1 = 30.973$, Ba- $K\alpha_1 = 32.194$ and La- $K\alpha_1 = 33.442$ keV) as tracers possessing three different valency states and being readily available as soluble chloride compounds.

1.3. Chalk

Chalk is a soft white limestone composed mainly of skeletal calcite that forms both a major aquifer and store of hydrocarbons (Håkansson *et al.*, 1974; Hancock, 1975; Scholle, 1977; Scholle *et al.*, 1983; Mortimore, 1990; Brooks and Glennie, 1987). In the UK the most important aquifer is formed by fractured chalk rock, generally considered a good example of a dual-porosity aquifer (Stossel and Hanor, 1975; Bibby, 1981; Black and Kipp, 1983). Groundwater flow is controlled by the secondary fracture porosity but diffusion of solutes into and out

of the fine matrix porosity plays an important part in the transport mechanism. The rock has the chemical quality of being almost pure calcium carbonate, which in the skeletal remains are organized predominately as crystals of low magnesian calcite.

The skeletal remains of the Coccolithophoridae form distinctively shaped particles the commonest of which is a calcite sphere ('coccosphere') of diameter 10-100 μm . Each coccosphere is originally composed of 7-20 rings or coccoliths 1-20 μm in diameter in turn formed of tablet-shaped calcite crystals called 'rays', 'plates', or 'laths' with diameters ranging from 0.17 to 2.8 μm . Other biogenic remains include Foraminifera representing 5-10% of the sample and some bivalve shells. The remains are lightly cemented and often have a significant part of their original structure intact creating a high interstitial void volume that, depending on the level of organisation of the crystals, yields matrix porosity values of between 20% and 45% even after diagenesis.

The microscopic nature of the porosity means that the matrix itself has a low permeability ($10^{-9} - 10^{-7} \text{ ms}^{-1}$, Hancock, 1993). The bulk permeability of the rock is substantially increased due to the presence of prolific sets of connected and usually orthogonal fractures. However the major control on the matrix permeability at the sub-fracture scale is the pore-size distribution, (Bear, 1972).

Chalk pore sizes have been investigated by Price *et al.* (1976) who describe distributions for 52 samples of English Chalk for different localities across the country from the results of mercury injection porosimetry (Ritter and Drake, 1945). Price *et al.* (1976) give the range of pore sizes as 0.012-100 μm , and the general mean pore size and standard deviation for all the samples as 0.49 and 0.2 μm . Specifically relevant for this study is their results for the Upper Chalk from

Southern England where they give values of 0.65 μm for the mean pore size and 0.14 μm for the standard deviation.

1.3.1. Experimental Sample

The sample of chalk used in this study was collected from a fresh rock fall at the excellent exposure at Birling Gap in East Sussex, England. The sample is of the Cuckmere beds, Seaford Chalk belonging to the Upper Chalk, taken from between 1m and 1.6 m above the stratigraphic marker provided by the Seven Sisters tabular flint band. This section is described as a uniform pure-white chalk of the *Micraster coranguinum* zone (Mortimore, 1997), and of the foraminiferal biozone *S. exscupta exscupta* (Bailey *et al.*, 1983). This uniformity makes it ideal for the use as a test material. Figure 2 shows a scanning electron microscope (SEM) image from the experimental chalk sample that highlights the porosity contribution in the matrix from the interstitial spaces between the coccolith fragments and the much larger void spaces left by the foraminiferal remains.

Figure 2

2. Sample Preparation

From the sample of chalk taken in the field several 25.4-mm diameter cores were cut and trimmed to 25.4 mm length to make in total twenty-seven experimental cores. The porosity of each was calculated using vacuum saturation and oven desiccation as described in the ISRM (1972) recommendations. Values ranged from 0.36 to 0.41 with an overall mean of 0.38, consistent with other porosity estimates (Hancock, 1993, Bloomfield *et al.*, 1995).

The cores were reduced as required to dimensions of 10 mm × 10 mm × 5 mm and all the samples then stored in a medium temperature oven (85°C) until taken for testing.

3. Tomographic Imaging of the Porosity Structure within Chalk

An investigation was performed, using a TXRF tracer to tomographically image the distribution of porosity at the millimetre scale in the chalk sample collected, exploiting the strong capillary forces generated by the fine interconnected pore spaces within the dry chalk. The relative strength of these forces for the different radii of capillaries formed by the interconnected pore spaces within the chalk are characterised by their matric potential (Case, 1994). In general the smaller the radius of the capillary then the larger the matric potential within it.

3.1. Experimental Procedure

A block of chalk was subjected to repeated tomographic scans after being saturated in steps of 20% to 80% of the fluid volume of the known (measured) porosity with high concentrations (25% by weight) of CsCl solution. Full saturation was not attempted due to uncertainty that all of the solution would be imbibed, given the decrease of capillary potential with degree of saturation. Each stage of tracer introduction was given 12-24 hours settling time before being scanned by TXRF to ensure an equilibrated fluid distribution within the pore structure. The measured volume of the tracer to be used was placed in a conical dish using a micro-fine syringe (accurate to 0.01 ml) into which the sample was placed (Figure 3) and covered. The capillary potential from the chalk is such that

the free tracer fluid in the dish was imbibed within a short time of coming into contact with the sample. The volume of the tracer applied was calculated on the basis of the porosity measurements made earlier.

Figure 3

Following the imbibing/distribution period the cover was removed from the dish and the sample immediately placed on the TEDDI translational stage for tomographic imaging across a complete 10 mm × 10 mm area section of the sample (Figure 4) using 11 × 11 nodes across a square grid. The pattern collection time at each node was 270 seconds, giving rise to a complete tomographic scan time of just over 9 hours.

Figure 4

3.2. Tomographic Results and Analysis

The tomographic spectra were adjusted, to compensate for the decay of the synchrotron beam current by normalising the fluorescence peak intensity to the integrated count intensity over the complete energy envelope so as to provide comparable fluorescence across the different spectra in the grid. Identification of the diffraction peaks (based on the ICDD Powder Diffraction File of d-spacings for calcite) indicated that the only significant crystalline phase present in the sample was calcite and the fluorescence peaks were clearly identified with Cs ($K_{\alpha} = 30.97$ keV, $K_{\beta} = 34.98$ keV). The resultant calcite and tracer concentrations are displayed (Figures 5 and 6) assuming proportionality with the respective peak intensities (i.e. assuming negligible variations due to multiple scattering or

absorption; Hall et al., 1998), using Kriging interpolation between nodes (Journel and Huijbregis, 1981; Oliver and Webster, 1990).

Figure 5

Figure 6

3.3. Discussion

Figure 6 gives a direct comparison between the images produced by diffraction and fluorescence for the same chalk sample. Two areas in particular, highlighted A and B, show obvious complementarity in the two images. Area A corresponds to both the highest intensity X-ray fluorescence region in the 80% saturation tomograph shown and the lowest calcite intensity in the TEDDI tomograph. Area B appears to be a similar region, although not as extreme as A. Both of these regions display what is expected for the interpretation of high porosity zones within the rock matrix.

Subsequent thin sectioning of the sample and analysis under a petrographic microscope tended to confirm this where regions of low matrix content corresponded with those of high fluorescence intensity. Additionally the relationship between the intensity of the tracer signal and the concentration of the solution has been tested separately using solutions corresponding to the likely concentration of tracer within the sample at the different levels of saturation (approximately 0.01 M to 0.1 M). The results indicate that a linear approximation provides a good local fit for this concentration range ($R^2 = 0.94$).

The 80% level of saturation used in the above comparison suggests that the areas A and B were generated by larger radii void spaces within the matrix such as created through foramaniferal remains as seen in Figure 2. If (a) the calcite TEDDI tomograph is taken to be representative of the rock matrix density throughout the sample and (b) the equivalent TXRF tomograph, of the sample saturated with a fluorescent tracer, is taken to be representative of the amount of connected pore space, then one would expect a strong negative correlation between the two images. Table I shows how the correlation coefficient between the calcite and fluorescence intensities increases (negatively) as the level of saturation increases.

Table I

From this trend the notion emerges that successive saturation images in Figure 5 represent accumulations of porosity distributions, with 20% corresponding to the initial filling of pore sizes up to a smaller diameter, similarly 40% up to a larger diameter and so on until 100% would envelope all capillary pores. Therefore to highlight this accumulation more clearly Figure 7 has been constructed so that each nodal intensity is expressed as a proportion of all saturations recorded at the same node, RC_p^n , i.e.:

$$RC_p^n = \frac{I_p^n}{I_{20\%}^n + I_{40\%}^n + I_{60\%}^n + I_{80\%}^n} \quad (4)$$

$$RC_p^n = \frac{I_p^n}{\sum_N I_p^N}$$

where I_p^n is the intensity at p percent for node n .

Figure 7

The assumption behind this approach is that all capillary pores, up to a radius determined by the level of saturation, are assumed to be filled with the tracer fluid. As the contribution of the capillaries to the total porosity depends on the square of the radius, a few larger radii pores will dominate the overall porosity and the recorded intensity for a node at particular level of saturation will mainly be constituted from the largest capillary diameter.

4. Conclusion

The experimental methods of TEDDI and TXRF have been described for use in investigating the porosity distribution within porous media at the laboratory scale. These measurements are non-destructive enabling repeat assays of the same experimental sample.

An illustration is given of the application of these methods in a hydrogeological context to highlight the porosity distribution within a sample of English Chalk. The results show how, by using the variation in matric potential generated by pores of different size, their relative distribution can be mapped from a grid of x-ray spectra. More specifically, TEDDI effectively maps the *total porosity* of the calcite matrix whereas TXRF effectively maps the *connected porosity* distributions for progressively higher levels of saturation and thereby also for progressively larger ranges of capillary sizes.

Acknowledgements

We would like to thank the Engineering and Physical Sciences Research Council, UK, for funding this research and the staff of the Daresbury Laboratory Synchrotron Radiation Source for their help and support.

5. References

Bailey, H. W., Gale, A. S., Mortimore, R. N., Swiecicki, A. and Wood, C. J: 1983, The Coniacian - Maastrichtian Stages of the United Kingdom, with particular reference to southern England, *Newsletters in Stratigraphy*, **12(1)**, 29-42.

Barnes, P., Colston, S. L., Craster, B., Hall, C., Jupe, A. C., Jacques, S. D. M., Cockcroft, J. K., Morgan, S., Johnson, M., O'Connor, D. and Bellotto, M. *J. Syncr. Rad.* **7(3)**, 117-177 (2000).

Bear, J: 1972, Dynamics of Fluids in Porous Media, American Elsevier Publishing Company, New York.

Bibby, R: 1981, Mass Transport of Solutes in Dual-Porosity Media, *Wat. Resources Res.*, **17**, 1075-1081.

Binley, A., Henry-Poulter, S. and Shaw, B: 1996a, Examination of solute transport in an undisturbed soil column using electrical resistance tomography., *Water Resources Research*, **32**, 763-769.

Binley, A., Shaw, B. and Henry-Poulter, S: 1996b, Flow pathways in porous media: Electrical resistance tomography and dye staining image verification., *Measurement Science Technology*, **7**, 384-390.

Black, J. H. and Kipp, K. L: 1983, Movement of Tracers Through a Dual-Porosity Media – Experiments and Modeling in the Cretaceous Chalk, England, *J. Hydrology*, **62**, 287-312.

Bloomfield, J. P., Brewerton, L. J. and Allen, D. J: 1995, Regional trends in matrix porosity and dry density of the Chalk of England, *Quarterly Journal of Engineering Geology*, Vol. **28**, S131-S142.

Brooks, J. and Glennie, K. W: 1987, Petroleum Geology of North West Europe. Proceedings of the 3rd Conference, Graham & Trotman, London, UK; 1987; 2 vol. xxiii+1219 pp.

Buras, B. and Gerward, L: 1989, Application of X-ray energy dispersive diffraction for characterization of materials under high pressure, *Prog. Cryst. Growth and Charact.*, **18**, 93-138.

Case, C. M: 1994, Physical Principles of Flow in Unsaturated Porous Media, Oxford Monographs on Geology and Geophysics No. 26, Oxford University Press Inc., New York.

Colston, S. L. Jupe, A. C. and Barnes, P: 2000, Synchrotron radiation tomographic energy-dispersive diffraction imaging. In *Radiation in Art and Archaeometry*, pp129-150, Eds. Creagh, D. C, and Bradley, D. A, Elsevier Science B.V.

Giessen, B. C. and Gordon, G. E: 1968, *Science*, **159**, 973.

Håkansson, E., Bromley, R., and Perch-Nielson, K: 1974, Maastrichtian chalk of north-west Europe – a pelagic shelf sediment. Pelagic sediments: On land and under water. pp211-23, *Spec. Pub. Int. Assoc. Sed.*, No. 1.

Hall, C., Barnes, P., Cockcroft, J. K., Colston, S. L., Hausermann, D., Jacques, S. D. M., Jupe, A. C. and Kunz, M: 1998, Synchrotron radiation energy-dispersive diffraction tomography, *Nucl. Instrum. & Meth. in Phys. Res. B* **140**, 253-257.

Hancock, J. M: 1975, The sequence of facies in the Upper Cretaceous of northern Europe compared with that in the western interior. The Cretaceous System in the Western Interior of North America, pp83-118, *Spec. Papers of Geol. Assoc. of Canada*, No.13.

Hancock, J. M: 1993, Modeling groundwater flow and transport in the Chalk, The Hydrogeology of the Chalk of North-West Europe, Oxford Science Pub., New York.

ISRM: 1972, Suggested Methods for Determining Water Content, Porosity, Density, Absorption and Related Properties, and Swelling and Slake-Durability Index Properties., International Society for Rock Mechanics Publications.

Journel, A. G. and Huijbregts, CH. J: 1981, Mining Geostatistics, Academic Press, New York.

Klug, H. P. and Alexander, L. E: 1974, X-ray diffraction procedures for polycrystalline and amorphous materials., 2nd Ed. J. Wiley & Sons, New York.

Liaw, H-K., Kulkarni, R., Chen, S. and Watson, A. T: 1996, Characterization of Fluid distributions in porous media by NMR techniques., *AICHE Journal*, Vol. **42**, No. **2**, 538-546.

Mortimore, R. N: 1997, The Chalk of Sussex and Kent, Geologists' Association Guide No.57.

Mortimore, R. N: 1990, The relationship between texture, density and strength of chalk. Chalk, pp109-32, Thomas Telford, London.

Oliver, M. A. and Webster, R: 1990, Kriging: a method of interpolation for geographical information system, *International Journal of Geographical Information Systems*, Vol. **4**, No. **3**, 313-332.

Olsen, P. A., Binley, A., Henry-Poulter, S. and Tych, W: 1999, Characterising solute transport in undisturbed soil cores using electrical and x-ray tomographic methods, *Hydrological Processes*, Vol. **13**, 211-221.

Price, M., Bird, M. J. and Foster, S. S. D: 1976, Chalk pore-size measurements and their significance, *Water Services*, **80**, 596-600.

Reichert, B., Hötzl, H. and Witthüser, K: 2001, Transport and Attenuation Processes in the Chalk Matrix., pp66-77, In *FRACFLOW Final Report: Contaminant transport, monitoring techniques, and remediation strategies in cross European fractured chalk.*, European Commission Contract No.: ENV4-CT97-0441.

Ritter, H. L. and Drake, L. C: 1945, Pore-size distribution in porous materials, *Ind. Engng. Chem. Anal.*, **17**, 782-786.

Scholle, P. A: 1977, Chalk diagenesis and its relation to petroleum exploration; oil from chalks, a modern miracle?, *Bull. Am. Assoc. Petrol. Geol.*, **61**, 982-1009.

Scholle, P. A., Arthur, M. A. and Ekdale, A. A: 1983, Pelagic environments, Carbonate Depositional Environments, pp619-91, Mem. Of the Am. Assoc. Petrol. Geol., No 33.

Stössel, R. K. and Hannor, J. S: 1975, A Nonsteady State Method for Determining Diffusion Coefficients in Porous Media, *J. Geophys. Res.*, **80**, 4979-4982.

Williams, G. M. and Higgo, J. J. W: 1994, In situ and laboratory investigations into contaminant migration, *J. Hydrol*, **159**, 1-25.

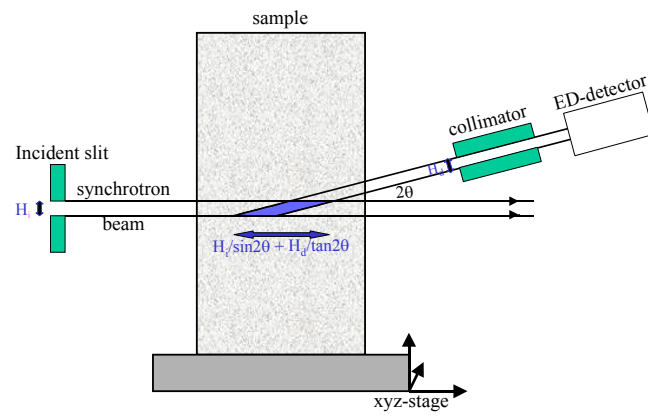


Figure 1

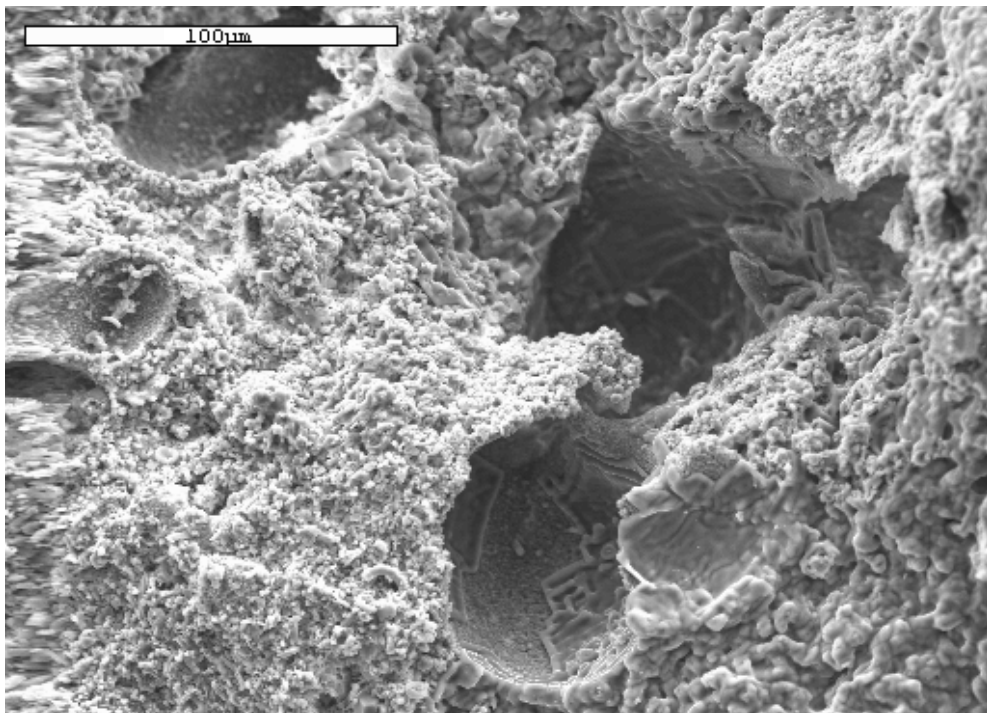


Figure 2

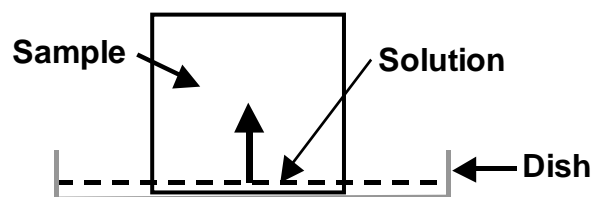


Figure 3

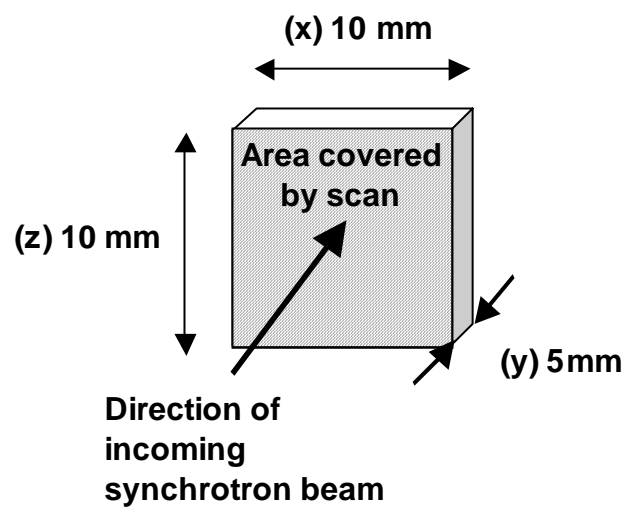


Figure 4

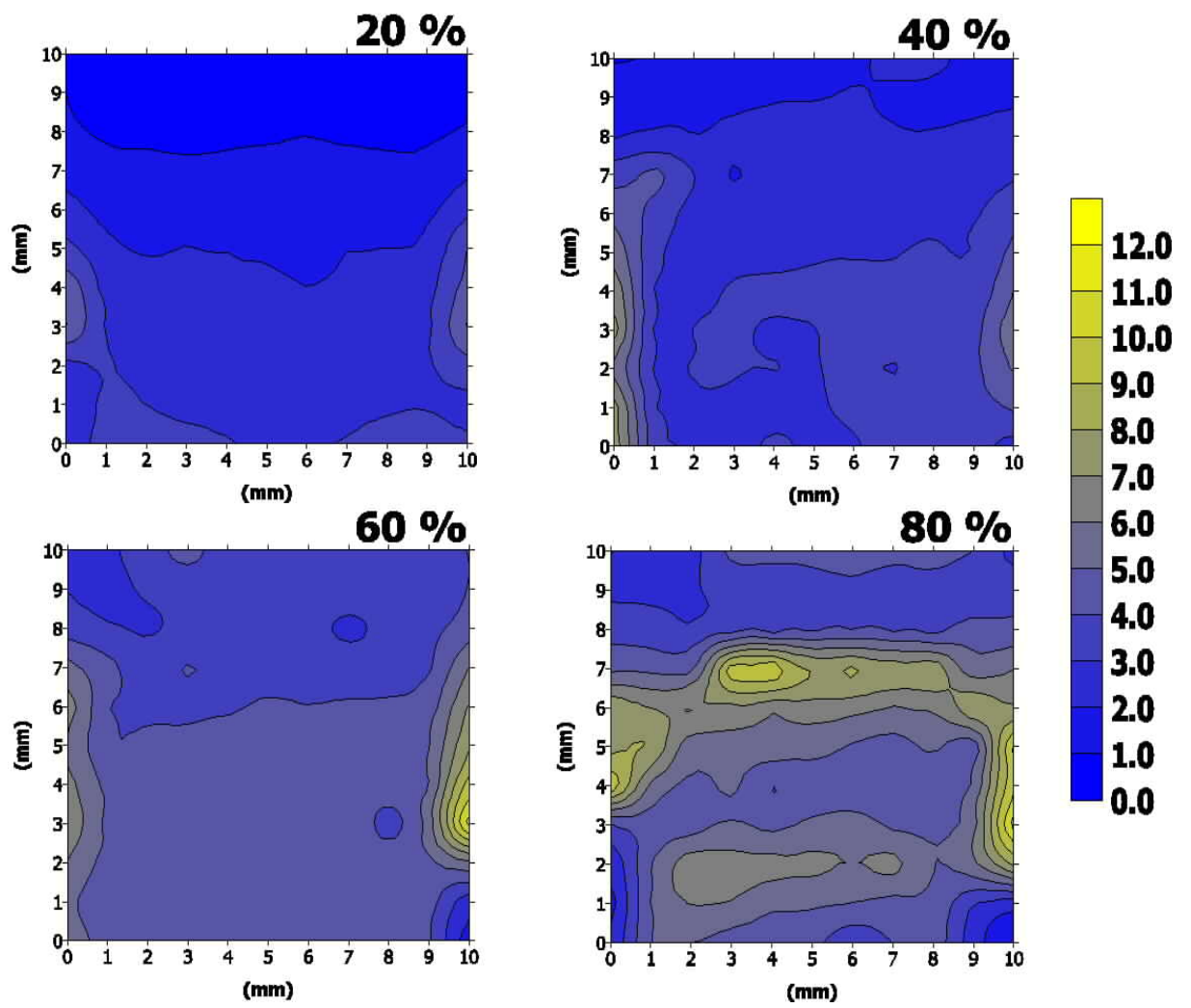


Figure 5

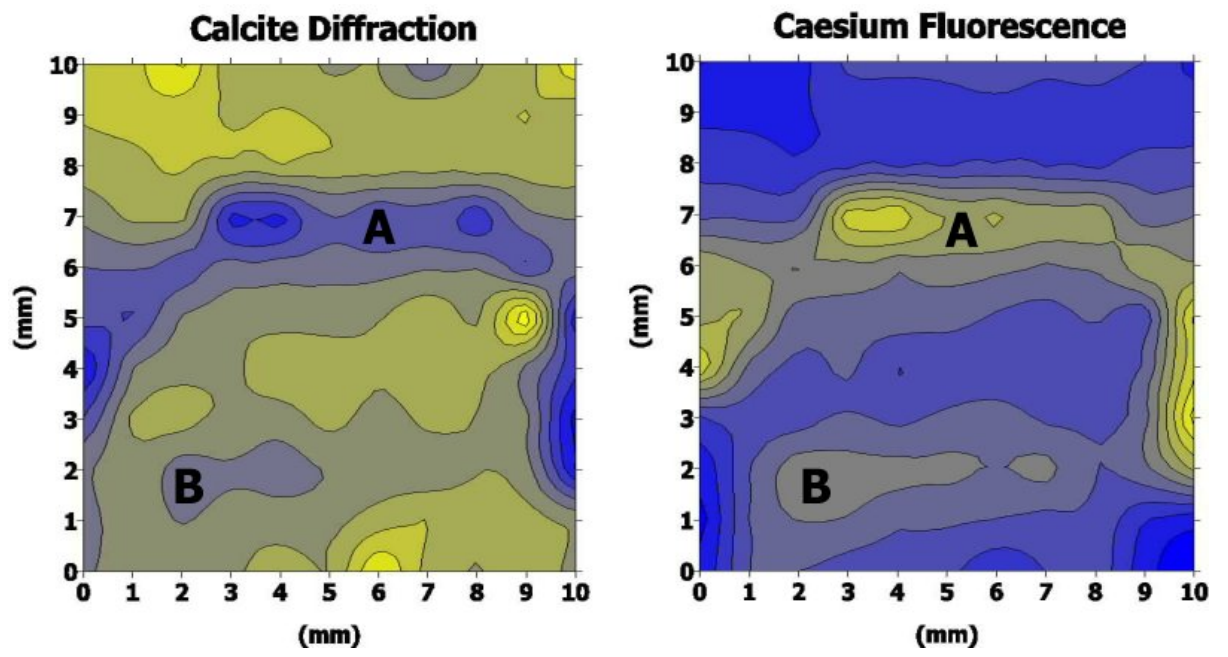


Figure 6

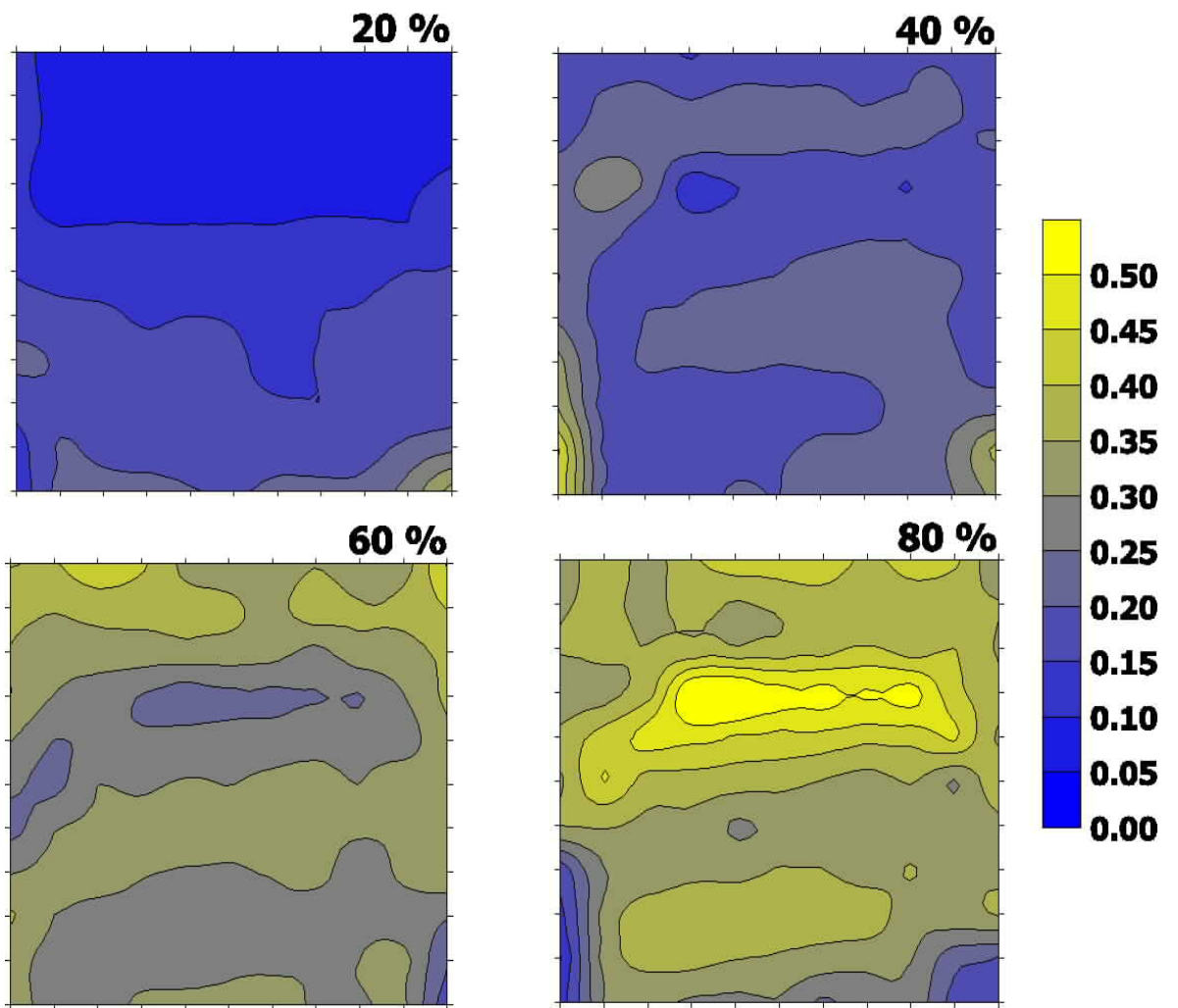


Figure 7

FIGURE CAPTIONS

Figure 1 Schematic of the TEDDI principle showing the lozenge-shaped sampling volume formed by the incident and diffracted synchrotron X-ray beam.

Figure 2 SEM image of Chalk sample from Birling Gap highlighting the large 20-40 μm spherical cavities seen in the matrix.

Figure 3 Schematic of the simple solution input procedure into the chalk sample.

Figure 4 Sample orientation with respect to the synchrotron beam during TEDDI analysis.

Figure 5 Kriged plots, interpolated over a square section arrays of 11×11 nodes and based on the intensity of the caesium $\text{K}\alpha$ fluorescence peak. These show the build up of tracer fluid in the chalk as the saturation level is increased through capillary action from the base of the sample.

Figure 6 Direct comparison between the TEDDI diffraction image of the calcite diffracted intensity and the TXRF fluorescence image for 80% saturation from Figure 5. The correlation is clear: for example, the regions A and B show high total porosity in the TEDDI image by absence of calcite diffraction and high connected porosity in the TRFA image by presence of the tracer fluid.

Figure 7 The relative contributions at each level of saturation (20%, 40%, 60% and 80%) of the caesium fluorescence intensities compared to the total sum at each node across all of the saturation levels.

<i>Level of Saturation</i>	<i>Correlation Coefficient</i>
20%	-0.417
40%	-0.480
60%	-0.510
80%	-0.819

Table I Correlation coefficient of calcite (1 0 4) diffraction intensity and caesium ($K\alpha$) fluorescence intensity at each level of saturation with the tracer fluid.